Second-harmonic generation from a Ag(111) surface at the interband transition region: Role of the dielectric function

C. M. Li, L. E. Urbach,* and H. L. Dai
Laboratory for Research on the Structure of Matter and Department of Chemistry, University of Pennsylvania, Philadelphia, Pennsylvania 19104
(Received 16 June 1993)

The azimuthal-angle dependence and the frequency dependence of second-harmonic generation (SHG) measured at the interband transition region of a Ag(111) surface have been examined using a theoretical model developed by Sipe, Moss, and van Driel [Phys. Rev. B **35**, 1129 (1987)]. The analyses of the experimental results provide strong evidence that the dramatic variation of the second-harmonic signal with frequency at $2\hbar\omega=3.87$ eV is primarily caused by the sharp change of the dielectric function. The dispersion of the dielectric function affects both the azimuthal angle and the frequency dependence through different radiation efficiencies of the isotropic and anisotropic components of the generated second-harmonic field. The observed SHG features at 3.9 eV can be adequately accounted for by the presence of the interband transitions, and it is not necessary to invoke other surface electronic transitions for their assignments.

I. INTRODUCTION

Since the first observations of second-harmonic generation (SHG) from a solid surface,[1,2] a number of studies have attempted to understand this phenomenon and applied it as a surface diagnostic technique.[3] Some recent investigations have concentrated on the measurement and understanding of the azimuthal-angle dependence[4-14] and the frequency dependence[4,11-18] of SHG from single crystal surfaces.

In the description of SHG at a vacuum-solid interface, there are two parameters, the dielectric function and the second-order susceptibility, that affect second-harmonic (SH) intensity through completely different mechanisms. The dielectric function ε, together with the light-incidence angle, determine the efficiency of the fundamental light penetrating into the surface and the second-harmonic light radiating into the vacuum. The second-order susceptibility $\chi^{(2)}$ manifests the intrinsic ability for the media to generate a SH field. The macroscopic parameters ε and $\chi^{(2)}$ both directly affect the SHG signal.[18]

The situation becomes interesting, as well as complicated, as one considers the "enhancement" of SHG due to resonance with electronic transitions. Resonance with electronic transitions is expected to increase $\chi^{(2)}$ and thereby enhance the SHG signal. However, electronic transitions also cause variations of ε, which may cause either enhancement or attenuation of the SHG signal.

Enhancement of $\chi^{(2)}$ due to resonance with surface electronic transitions has been unambiguously shown.[15,16] A strong enhancement of SHG signal on a Ag(110) surface was observed at $\hbar\omega=1.7$ eV and proven to be due to resonance with a surface state transition through symmetry selection rules.[15] The presence of the surface state transition has negligible effect on ε. Enhancement in SHG comes primarily from increases in $\chi^{(2)}$.

A second enhancement of SHG at $2\hbar\omega=3.9$ eV was also identified on both the Ag(111) (Refs. 12, 14, and 17) and Ag(110) (Ref. 15) surfaces. The energy of this enhancement is in the proximity of the L_3-$L_{2'}$, and the $L_{2'}$-L_1 interband transitions. These transitions also give rise to the silver plasmon frequency of 3.9 eV.[19] It is unclear how the interband transitions would affect the SHG since it can affect both $\chi^{(2)}$ and ε. Several possibilities on the nature of the electronic transition that originates this enhancement feature have been proposed.[12,14,17,18]

In a study by Giesen *et al.*, SH signal was measured on a Ag(111) surface from $2\hbar\omega=3.73$ to 4 eV.[17] A peak at 3.85 eV was observed. This result was consistent with the two-photon photoemission measurements by the same authors that showed a resonance feature at 3.84 eV. They have assigned this feature observed on the Ag(111) surface to resonance with a transition from an occupied surface state A at $\bar{\Gamma}$ to an unoccupied image state I. Following this proposal, in a recent work Bradley *et al.*[12] have suggested that the similar resonance feature observed on a Ag(111) surface under ultrahigh vacuum as well as submerged in an electrolyte solution was a result from resonant enhancement by either a transition from the occupied surface state A to the bulk sp band or the A-I transition.

In relating the observed SHG peaks to resonance with electronic transitions, these previous works have not included in their consideration the possible effect on SHG caused by the dramatic variation of the dielectric function at this energy region due to the presence of the interband transitions. The dielectric function in the 3.6–4.4-eV or 280–340-nm region[20] is shown in Fig. 1. Both the real and imaginary parts have strong frequency dependence and are close to zero at 3.9 eV (320 nm). The radiation efficiency of the SHG signal could be greatly affected by the dielectric function in this energy region.[14,18]

In order to address the issues discussed above, we have

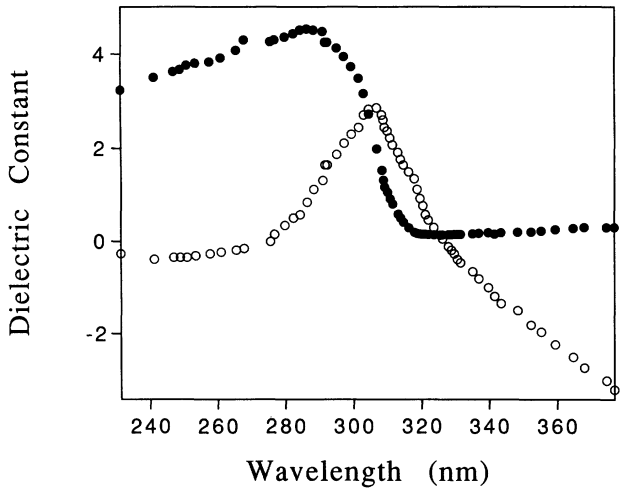

FIG. 1. The dielectric function of Ag at the interband transition region from Ref. 20. The open circles are the real part and the solid circles the imaginary part.

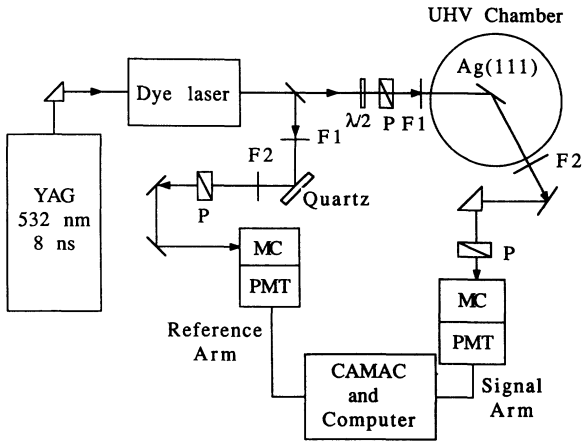

FIG. 2. Experimental setup. P refers to polarizer and MC monochrometer. $F1$ refers to the filters that block SH light and transmit the fundamental light, while $F2$ refers to the filters that block the fundamental light and transmit the SH light.

measured azimuthal-angle dependence together with frequency dependence on a Ag(111) surface at the interband transition region using different light polarization conditions. The isotropic and anisotropic components of SHG with different light polarization were analyzed by using a phenomenological model developed by Sipe, Moss, and van Driel (the SMD model),[4] which will be described in detail in a following section. Through model analyses of SHG from this clean Ag surface, we will show that the dramatic changes in the SHG in the interband transition region can be attributed to primarily the strong dispersion of the dielectric function $\varepsilon(2\omega)$, and the previously proposed assignments of the observed SHG peaks to resonances with transitions involving surface electronic states are not substantiated.

II. EXPERIMENT

All experiments reported here were performed with a Ag single crystal in the UHV chamber, which had a base pressure of 8×10^{-11} Torr. The chamber was equipped with a mass spectrometer and an Auger electron spectrometer. A manipulator allowed the Ag crystal to be rotated around its surface normal. The sample could be heated up to 450 °C with electron bombardment or cooled down to 90 K with liquid nitrogen. Each time before an experiment, the crystal was cleaned by Ar^+ sputtering and followed by annealing to 450 °C.

The 532-nm output of a 20-Hz pulsed Nd:YAG (yttrium aluminum garnet) laser (Quantel 581C) was used to pump a pulsed dye laser (Quanta-Ray PDL-2) to generate the fundamental light. The tuning range of the dye laser spanned from about 580 to 900 nm. The peak power was approximately 50 MW/cm^2 with a pulse duration full width at half maximum of 8 ns.

In the experimental setup shown in Fig. 2, the dye laser pulse passed through a half-wave plate and a polarizer to set the polarization direction. A UV cutoff filter was placed in the laser-beam path before the chamber to remove any SH light generated by the optics. The light-incidence angle was set to 60°. The laser beam reflected off the crystal exited the UHV chamber through a sapphire window and then passed through several Corning 7-54 filters which removed the fundamental beam. The remaining SH signal was then passed through a polarizer for polarization selection. The polarized SH signal was detected by a photomultiplier and processed by a microcomputer equipped with a CAMAC gated detection system for signal averaging. A fraction ($\sim4\%$) of the fundamental light was split off and sent onto a quartz plate. SHG from the quartz surface was used as a reference to correct for laser intensity fluctuation.

III. EXPERIMENTAL RESULTS

The azimuthal-angle dependence of SHG from Ag(111) was measured with different polarization conditions at several wavelengths in the interband transition region.

Based on the threefold crystalline symmetry of the (111) surface, the following expressions describe the azimuthal-angle dependence of SHG:

$$I_{pp}=|(I_{pp}^{\rm iso})^{1/2}+e^{i\delta_{pp}}(I_{pp}^{\rm aniso})^{1/2}\cos(3\phi)|^2 , \quad (1)$$

$$I_{sp}=|(I_{sp}^{\rm iso})^{1/2}+e^{i\delta_{sp}}(I_{sp}^{\rm aniso})^{1/2}\cos(3\phi)|^2 , \quad (2)$$

$$I_{ss}=I_{ss}^{\rm aniso}|\sin(3\phi)|^2 , \quad (3)$$

where, for example, sp refers to s-polarized fundamental light and p-polarized SH light and $I_{sp}^{\rm iso}$ and $I_{sp}^{\rm aniso}$ are defined as the isotropic and anisotropic components of the sp-polarized light. δ is the phase angle between the isotropic and anisotropic components. The azimuthal angle ϕ is defined as the angle between the light-incidence plane and the $[2\bar{1}\,\bar{1}]$ direction of the Ag crystal.

Figure 3 shows the azimuthal-angle dependence of I_{pp} at seven different SH wavelengths. The overall SHG signal is the strongest at 320 nm. The azimuthal-angle dependence becomes increasingly isotropic as the SH wavelength approaches 320 nm, which is shown by its pattern change from a six-peak symmetry to a three-peak symmetry in a range of 360°.

The azimuthal-angle dependences of I_{pp} were fitted by Eq. (1) with three fitting parameters $I_{pp}^{\rm iso}$, $I_{pp}^{\rm aniso}$, and $|\delta_{pp}|$. The fitting results for $I_{pp}^{\rm aniso}$ are displayed as a function of SH wavelength in Fig. 4. There is a dip at 322.5 nm. $I_{pp}^{\rm aniso}$ actually displays an attenuation, not enhancement, in the interband transition region. The ratio $(I_{pp}^{\rm iso}/I_{pp}^{\rm aniso})^{1/2}$ and the phase angle $|\delta_{pp}|$, are listed in Table I. The ratio $(I_{pp}^{\rm iso}/I_{pp}^{\rm aniso})^{1/2}$, which depicts the relative magnitude of isotropic versus anisotropic components, peaks at 322.5 nm. One can also see the trend of the phase angle $|\delta_{pp}|$—it becomes smaller as the wavelength approaches 322.5 nm. However, the significance of this pattern as well as the sign of δ_{pp} is not clear.

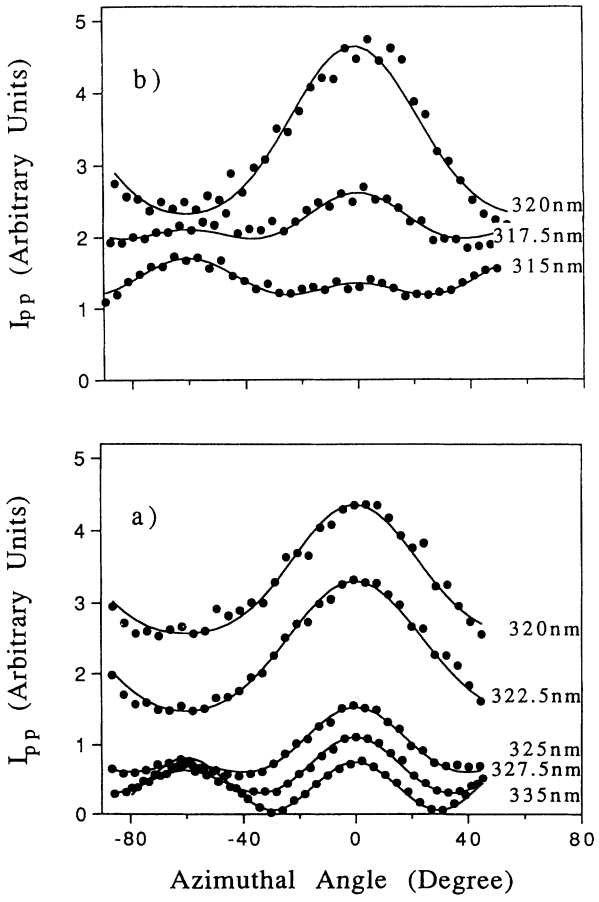

FIG. 3. Azimuthal-angle dependence of I_{pp} at different wavelengths in the interband transition region. The points are experimental data. The curves are the nonlinear least-squares fit to Eq. (1). Each curve is labeled by the SH wavelength. The data are shown in two panels, with the same intensity unit to prevent overlapping.

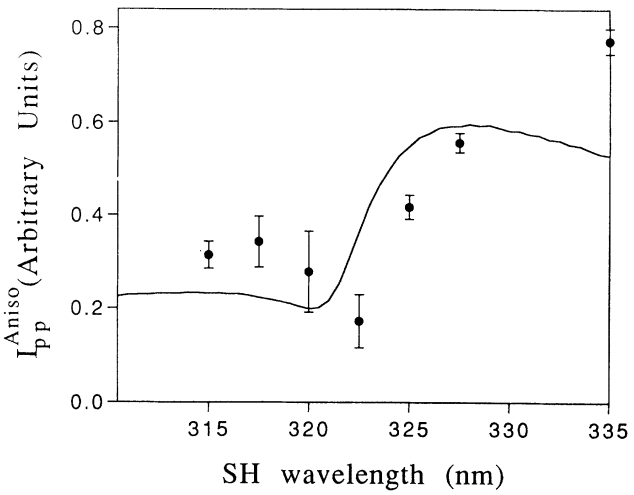

FIG. 4. Frequency dependence of the anisotropic component of I_{pp} noted as $I_{pp}^{\rm aniso}$. The points are from pattern analysis of the measurement shown in Fig. 3. The curve is a least-squares fit to Eq. (16) in direct proportion to the radiation efficiency $|F_c A_p|^2$.

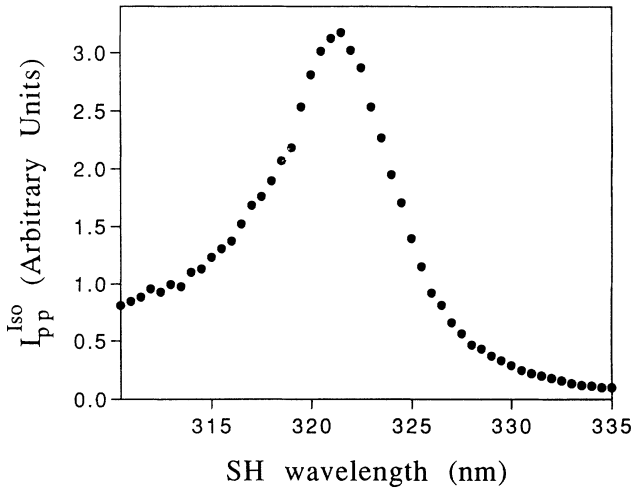

FIG. 5. Frequency dependence of the isotropic component of I_{pp} noted as $I_{pp}^{\rm iso}$ from direct measurement of I_{pp} at $3\phi=90°$.

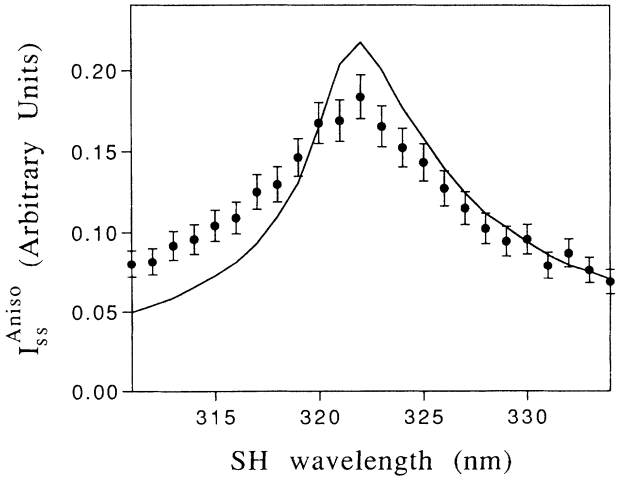

FIG. 6. Frequency dependence of the anisotropic component of I_{ss} noted as $I_{ss}^{\rm aniso}$. The points are experimental data obtained at $3\phi=90°$. The curve is a least-squares fit to Eq. (17) in direct proportion to the radiation efficiency $|A_s|^2$.

TABLE I. The ratio of the isotropic and the anisotropic components of I_{pp} and the phase angle $|\delta_{pp}|$ at different wavelengths. The results are obtained from analyzing the azimuthal angle dependence pattern of I_{pp}.

SH wavelength (nm)	$\lvert I_{pp}^{iso}/I_{pp}^{aniso}\rvert^{1/2}$	$\lvert\delta_{pp}\rvert$
315	1.9±0.1	98°±1°
317.5	2.4±0.1	81°±1°
320	3.3±0.5	54°±6°
320	3.5±0.5	61°±4°
322.5	3.4±0.5	44°±8°
325	1.3±0.1	68°±1°
327.5	0.58±0.02	74°±1°
335	0.07±0.07	95°±2°

The azimuthal-angle dependence of I_{ss} was measured at 320 nm only. It displays a six-peak symmetry pattern with 100% modulation and one of the zero-intensity valley centered at 0°. This azimuthal-angle dependence can be well described by Eq. (3) and indicates that there is no isotropic component for I_{ss} at 320 nm.

The frequency dependence of the isotropic and the anisotropic components of the SH intensity under various polarization conditions were also directly measured. The frequency dependence of I_{pp}^{iso} was obtained by measuring the frequency dependence of I_{pp} at $3\phi=90°$ (Fig. 5). Based on Eq. (1), at this angle $I_{pp}=I_{pp}^{iso}$. Apparently, I_{pp}^{iso} is enhanced in the interband transition region.

Based on Eq. (3), I_{ss}^{aniso} can be measured as I_{ss} at $3\phi=90°$. The frequency dependence of I_{ss}^{aniso} is shown in Fig. 6. An enhancement was observed. This enhancement in I_{ss}^{aniso} is exactly the opposite to the attenuation observed in I_{pp}^{aniso}.

Based on Eq. (2), the frequency dependence of I_{sp}^{iso} was measured as I_{sp} at $3\phi=90°$. I_{sp}^{iso} appears to be two orders of magnitude smaller than I_{pp}^{iso} and also shows an enhancement behavior (Fig. 7).

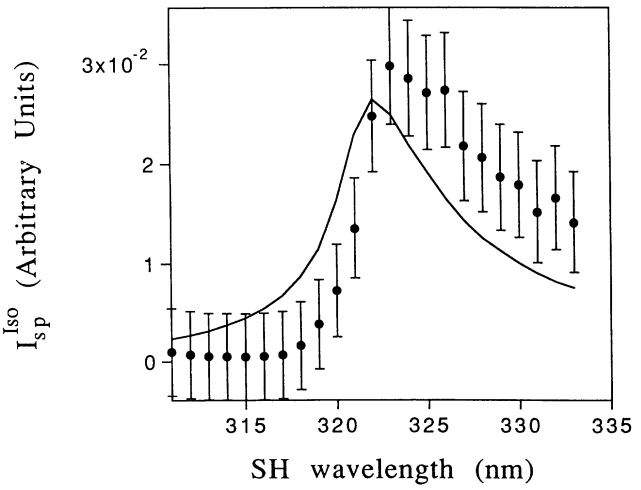

FIG. 7. Frequency dependence of the isotropic component of I_{sp} noted as I_{sp}^{iso}. The points are experimental data obtained at $3\phi=90°$. The curve is a least-squares fit to Eq. (15) in direct proportion to the radiation efficiency $|F_s A_p|^2$ only.

Also directly measured were the frequency dependence of I_{pp} and I_{sp} at $\phi=0°$, where the isotropic component and the anisotropic component coexist. The results are shown in Figs. 8(a) and 8(b). The frequency dependence of $I_{pp}(\phi=0°)$ shows a peak at 321 nm, while that of $I_{sp}(\phi=0°)$ has a dip at 321 nm.

IV. THEORETICAL MODEL

Our analysis of the azimuthal angle and the frequency dependence of SHG is based on a model presented by Sipe, Moss, and van Driel originally laid out for a variety of crystalline surfaces.[4] In the SMD model, SHG at a vacuum-(111) interface has two origins: the surface with a threefold symmetry and the bulk of a cubic centrosymmetric crystal. For the bulk contribution, the effective polarization includes magnetic-dipole and electric-quadrupole responses. For the surface contribution, this model considered an effective surface dipole due to the discontinuity in the normal component of the electric field and inversion symmetry breaking at the surface.[2,21]

Both of these effects were depicted by an effective surface dipole, which generates nonlinear susceptibility components of different directions, χ_{ijk}'s. This model as-

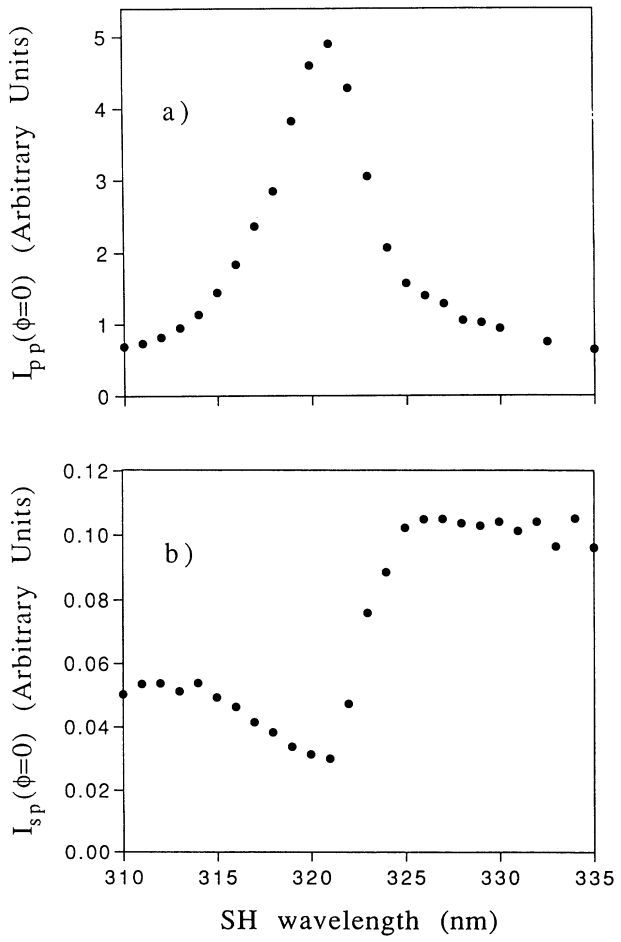

FIG. 8. (a) Frequency dependence of I_{pp} at $3\phi=0$. (b) Frequency dependence of I_{sp} at $3\phi=0$.

sumed that the dielectric constant of the crystal surface is the same as that of the bulk.

Based on these considerations, Sipe, Moss, and van Driel derived the azimuthal-angle dependence of the *pp*-, *sp*-, and *ss*-polarized SH intensities from the (111) surface as

$$I_{pp}=\frac{c}{8\pi}(t_pE_0)^4A_p^2[a_{pp}+c_{pp}\cos(3\phi)]^2 , \tag{4}$$

$$I_{sp}=\frac{c}{8\pi}(t_sE_0)^4A_p^2[a_{sp}+c_{sp}\cos(3\phi)]^2 , \tag{5}$$

$$I_{ss}=\frac{c}{8\pi}(t_sE_0)^4A_s^2[b_{ss}\sin(3\phi)]^2 . \tag{6}$$

Here, t_p and t_s are the usual Fresnel coefficients for *p*- and *s*- polarized fundamental light, respectively. A_p and A_s are the Fresnel coefficients for *p*- and *s*-polarized SH light multiplied by a factor of $2\pi/\cos\theta$. The parameters a, b, and c are functions of bulk (γ and ζ) and surface (χ_{ijk}'s) nonlinear susceptibilities and dielectric functions $\varepsilon(\omega)$ and $\varepsilon(2\omega)$. The original forms of a, b, and c can be found in Ref. 4. The simplified expressions in the limit of large $|\varepsilon(\omega)|$ (Ref. 10) and on the condition of $|\varepsilon(\omega)|\gg|\varepsilon(2\omega)|$ are given as follows:

$$a_{pp}=\frac{i2\omega}{c}\{\tfrac{4}{3}F_s\eta+F_s[\varepsilon(2\omega)\chi_{zxx}^{(2)}+\gamma] +\varepsilon(2\omega)F_sf_s^2\chi_{zzz}^{(2)}-2f_sF_c\chi_{xzx}^{(2)}\} , \tag{7}$$

$$c_{pp}=-\frac{i2\omega}{c}F_c\left\{\frac{2(2)^{1/2}}{3}\eta-\chi_{xxx}^{(2)}\right\} , \tag{8}$$

$$a_{sp}=\frac{i2\omega}{c}\{\tfrac{4}{3}F_s\eta+F_s[\varepsilon(2\omega)\chi_{zxx}^{(2)}+\gamma]\} , \tag{9}$$

$$c_{sp}=\frac{i2\omega}{c}F_c\left\{\frac{2(2)^{1/2}}{3}\eta-\chi_{xxx}^{(2)}\right\} , \tag{10}$$

and

$$b_{ss}=-\frac{i2\omega}{c}\left\{\frac{2(2)^{1/2}}{3}\eta-\chi_{xxx}^{(2)}\right\} , \tag{11}$$

where $\eta\approx\zeta/8f_c$.

From the above equations, it is not hard to find the following relations among the parameters:

$$a_{pp}=a_{sp}+\frac{i2\omega}{c}\varepsilon(2\omega)F_sf_s^2\chi_{zzz}^{(2)}-\frac{i4\omega}{c}f_sF_c\chi_{xzx}^{(2)} , \tag{12}$$

and

$$c_{pp}=-c_{sp}=F_cb_{ss} . \tag{13}$$

In Eqs. (7)–(11), f_s, f_c, t_p, and t_s are functions of the incident angle and the dielectric function $\varepsilon(\omega)$, and F_s, F_c, A_p, and A_s are functions of the incident angle and the dielectric function $\varepsilon(2\omega)$. The dielectric function of Ag, including that around the interband transition region, was obtained from Ref. 20, which enabled us to calculate f_s, f_c, t_p, t_s, F_s, F_c, A_p, and A_s. It was found that the functions associated with the dielectric function $\varepsilon(2\omega)$, such as F_s, F_c, A_p, and A_s, are strongly frequency dependent because of the strong dispersion of $\varepsilon(2\omega)$ in the interband transition angle. On the other hand, f_s, f_c, t_p, and t_s are weakly frequency dependent with a less than 10% variation because of the weak frequency dependence of $\varepsilon(\omega)$.

V. DATA ANALYSIS AND DISCUSSION

In this section, we will discuss the origins for the frequency dependence of SHG. The analyses of the experimental data based on the SMD model will allow us to examine the effect of dielectric constant ε versus nonlinear susceptibility $\chi^{(2)}$.

The frequency dependence of the isotropic and the anisotropic components shows dramatically different behaviors in the interband transition region: some are enhanced and some attenuated. Even for the enhanced ones, the enhancement features are different in shape. It is important to find out the mechanism responsible for these behaviors.

The SMD model explicitly shows how nonlinear susceptibility and dielectric constants affect the SHG. Interpretation of the experimental data according to this model allows us to determine the relative importance of ε versus $\chi^{(2)}$. Considering the dramatic variation of $\varepsilon(2\omega)$ at the interband transition region, we first examine the effect of $\varepsilon(2\omega)$ on the isotropic and anisotropic components separately in the following subsections.

A. The frequency dependence of I_{pp}^{iso}

In the SMD model, there are too many unknown parameters in the analytical expression for I_{pp}^{iso} to be determined separately by a nonlinear least-squares fit of the data. However, one can still appreciate the importance of the dielectric function $\varepsilon(2\omega)$ through a semiquantitative analysis. I_{pp}^{iso} can be rearranged as

$$I_{pp}^{iso}=T_p^2|F_sA_pa_{bulk}+\varepsilon(2\omega)F_sA_pa_{surface,\perp} +F_cA_pa_{surface,\parallel}|^2 \tag{14}$$

with the following definitions:

$$T_p\equiv\left|\frac{\omega}{(2\pi c)^{1/2}}(t_pE_0)^2\right| , \quad a_{bulk}\equiv\tfrac{4}{3}\eta+\gamma ,$$

$$a_{surface,\perp}\equiv\chi_{zxx}^{(2)}+f_s^2\chi_{zzz}^{(2)} , \quad a_{surface,\parallel}\equiv-2f_s\chi_{xzx}^{(2)} .$$

In the above expression, T_p has a negligible frequency dependence ($\sim$10% variation). The terms F_sA_p, $\varepsilon(2\omega)F_sA_p$, and F_cA_p, which represent radiation efficiencies of SH fields generated from three different sources, are strongly frequency dependent because they are functions of $\varepsilon(2\omega)$. The second-order susceptibility components are regrouped so that those with the same radiation efficiency are put together. For example, the SH fields from the two bulk components η (proportional to ζ) and γ have the same radiation efficiency represented by F_sA_p. These two components are regrouped into a_{bulk}.

The squares of F_sA_p, $\varepsilon(2\omega)F_sA_p$, and F_cA_p, which

correspond to the radiation efficiencies of the SH intensities, are displayed in Fig. 9. Apparently, they all have strong frequency dependence with their shapes strongly correlated to the frequency dependence of $I_{pp}^{\rm iso}$. Even without a detailed calculation, one can perceive that the frequency dependence of the radiation efficiencies is the primary cause for the observed enhancement in $I_{pp}^{\rm iso}$ before considering the possible frequency dependence in the second-order susceptibility components.

B. The frequency dependence of $I_{sp}^{\rm iso}$

The expression of $I_{sp}^{\rm iso}$ in the SMD model is simpler than that of $I_{pp}^{\rm iso}$ because it contains less source terms. $I_{sp}^{\rm iso}$ can be expressed as

$$I_{sp}^{\rm iso}=T_s^2|F_s A_p a_{\rm bulk}+\varepsilon(2\omega)F_s A_p \chi_{zxx}^{(2)}|^2 , \tag{15}$$

with T_s defined as

$$T_s \equiv \left| \frac{\omega}{(2\pi c)^{1/2}}(t_s E_0)^2 \right| .$$

T_s has a negative frequency dependence like T_p. $I_{sp}^{\rm iso}$ contains two kinds of SH source terms, the bulk term $a_{\rm bulk}$ and the surface term $\chi_{zxx}^{(2)}$, with the radiation efficiency functions $F_s A_p$ and $\varepsilon(2\omega)F_s A_p$, respectively. For simplification, the surface term $\chi_{zxx}^{(2)}$ is neglected based on the result of the jellium-model calculations, in which $\chi_{zxx}^{(2)}=0$.[10,22–24] However, considering that Ag is not a perfect jellium metal, one may need further justifications for this simplification. In fact, the following analysis does provide a strong piece of evidence that the simplification $\chi_{zxx}^{(2)}\sim 0$ is reasonable as well as the idea that the frequency dependence of the SH intensity is dominated by $\varepsilon(2\omega)$.

After neglecting the surface term, the frequency dependence of $I_{sp}^{\rm iso}$ should come from $a_{\rm bulk}$ and/or the radiation efficiency function $F_s A_p$. $|F_s A_p|^2$ shown in Fig. 9(a) resembles the frequency dependence of $I_{sp}^{\rm iso}$ in shape. A fit of $I_{sp}^{\rm iso}$ to Eq. (15) without the surface term is shown in Fig. 7. This fit involves only one free parameter $|T_s a_{\rm bulk}|^2$ and does reproduce the frequency dependence of $I_{sp}^{\rm iso}$ reasonably well. The success of this fit reveals that the frequency dependence of $I_{sp}^{\rm iso}$ comes mainly from that of the radiation efficiency $|F_s A_p|^2$. The dispersion of $\varepsilon(2\omega)$ overwhelmingly dominates over the possible frequency dependence of $\chi^{(2)}$ in the SHG. Furthermore, it supports the simplification that the surface term of $I_{sp}^{\rm iso}$ is negligible. Indeed, the surface term radiation efficiency $|\varepsilon(2\omega)F_s A_p|^2$ [Fig. 9(b)] does not resemble the frequency dependence of $I_{sp}^{\rm iso}$. If $I_{sp}^{\rm iso}$ contained much surface contribution, a different frequency dependence of $I_{sp}^{\rm iso}$ would have appeared.

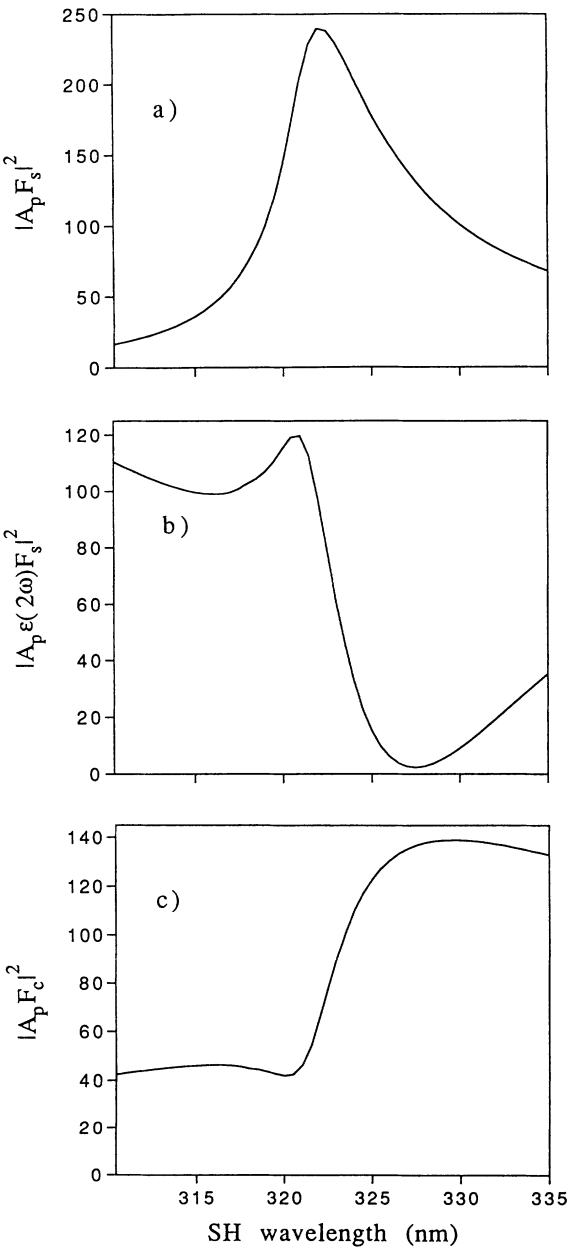

FIG. 9. Frequency dependence of the radiation efficiency functions (a) $|F_s A_p|^2$, (b) $|\varepsilon(2\omega)F_s A_p|^2$, and (c) $|F_c A_p|^2$.

C. The frequency dependence of $I_{pp}^{\rm aniso}$

Unlike $I_{pp}^{\rm iso}$ and $I_{sp}^{\rm iso}$, the expression of $I_{pp}^{\rm aniso}$ contains only one type of radiation efficiency,

$$I_{pp}^{\rm aniso}=T_p^2\left|F_c A_p\left\{-\eta\frac{2^{3/2}}{3}-\chi_{xxx}^{(2)}\right\}\right|^2 . \tag{16}$$

The SH fields generated by both bulk and surface sources have the same radiation efficiency behavior represented by $F_c A_p$. $I_{pp}^{\rm aniso}$ is directly proportional to $|F_c A_p|^2$. In fact, a fit of $I_{pp}^{\rm aniso}$ to Eq. (16) with only one free parameter reproduces the main features of the frequency dependence (Fig. 4). The frequency dependence of the radiation efficiency alone can reproduce that of $I_{pp}^{\rm aniso}$. This is one more piece of evidence that $\varepsilon(2\omega)$ is primarily responsible for the frequency-dependent behavior in the interband transition region.

D. The frequency dependence of I_{ss}^{aniso}

Similar to I_{ss}^{aniso}, the expression of I_{ss}^{aniso} also has only one type of radiation efficiency function

$$I_{ss}^{aniso}=T_s^2\left|A_s\left\{-\eta\frac{2(2)^{1/2}}{3}-\chi_{xxx}^{(2)}\right\}\right|^2 . \quad (17)$$

I_{ss}^{aniso} should vary with the radiation efficiency function $|A_s|^2$. Indeed, this is borne out in a one-free-parameter fit of I_{ss}^{aniso} to Eq. (17) shown in Fig. 6. The success of the fit again supports the deduction that the frequency dependence of the SH intensities comes mainly from the dispersion of $\varepsilon(2\omega)$.

E. Comparison of the frequency dependence of I_{pp} and I_{sp} at $\phi=0$

As shown in Fig. 8, the frequency dependence of I_{pp} at $\phi=0$ shows a peak but that of I_{sp} shows a valley in the interband transition region. To the best of our knowledge, this is the first time that an attenuation feature in SHG is observed in the energy region of an electronic excitation. According to Eqs. (1) and (2), the *pp*-polarized and *sp*-polarized SHG intensity at the azimuthal angle $\phi=0$ should have the following expressions:

$$I_{pp}(\phi=0)=[(I_{pp}^{iso})^{1/2}+e^{i\delta}(I_{pp}^{aniso})^{1/2}]^2 , \quad (18)$$

$$I_{sp}(\phi=0)=[(I_{sp}^{iso})^{1/2}+e^{i\delta}(I_{sp}^{aniso})^{1/2}]^2 . \quad (19)$$

The overall spectral shape of $I_{pp}(\phi=0)$ or $I_{sp}(\phi=0)$ is determined by the relative magnitude of the isotropic versus the anisotropic components. The isotropic components I_{pp}^{iso} and I_{sp}^{iso} have their peaks around 320 nm while the anisotropic components I_{pp}^{aniso} and I_{sp}^{aniso} have their dips at 320 nm. Therefore, for either $I_{pp}(\phi=0)$ or $I_{sp}(\phi=0)$, if the isotropic component dominates, the spectral feature will show a peak. If the anisotropic component dominates, it will show a valley.

According to the values of $|I_{pp}^{iso}/I_{pp}^{aniso}|^{1/2}$ listed in Table I, the ratio $I_{pp}^{iso}/I_{pp}^{aniso}$ is ~ 12 at the center of the interband transition region. I_{pp}^{iso} should dominate the frequency dependence of $I_{pp}(\phi=0)$ and indeed, a peak is shown in the frequency dependence of $I_{pp}(\phi=0)$ in Fig. 8(a).

In order to understand the frequency dependence of I_{sp}, we also have to examine the ratio $I_{sp}^{iso}/I_{sp}^{aniso}$, which can be determined by the following relation:

$$I_{sp}^{iso}/I_{sp}^{aniso}=|a_{sp}/c_{sp}|^2$$
$$=|a_{sp}/a_{pp}|^2|a_{pp}/c_{pp}|^2|c_{pp}/c_{sp}|^2 . \quad (20)$$

From Eq. (13), we have $|c_{pp}/c_{sp}|=1$. According to Eqs. (4) and (5), the second ratio $|a_{sp}/a_{pp}|^2$ is equal to $(t_p/t_s)^4(I_{sp}^{iso}/I_{pp}^{iso})$. The ratio t_p/t_s is calculated to be approximately 2.0 based on the dielectric function from Ref. 12. The ratio $I_{sp}^{iso}/I_{pp}^{iso}$ has been measured to be about 0.002 at 320 nm. Therefore, the ratio $|a_{sp}/a_{pp}|^2$ is calculated to be 0.03. It is known from Table I that $|a_{pp}/c_{pp}|^2=I_{pp}^{iso}/I_{pp}^{aniso}\sim 12$ at 320 nm. Combining all three factors, we obtain $I_{sp}^{iso}/I_{sp}^{aniso}\sim 0.4$. This value indicates that I_{sp}^{aniso} makes a larger contribution than I_{sp}^{iso} to I_{sp}. Note that both ratios $I_{sp}^{iso}/I_{pp}^{iso}$ and $I_{pp}^{iso}/I_{pp}^{aniso}$ are either measured or estimated at 320 nm. Since this is the center of the interband transition region, the shape of the I_{sp}^{aniso} frequency dependence should dominate and an attenuated feature appears in the frequency dependence of $I_{sp}(\phi=0)$.

F. The effect of ε versus $\chi^{(2)}$ in the interband transition region

The above analysis of the frequency dependence of each isotropic or anisotropic SHG intensity component under different polarization conditions consistently shows that the frequency dependence in radiation efficiency induced by the dispersion of the dielectric function $\varepsilon(2\omega)$ is the primary cause for the observed frequency-dependent behaviors in SHG in the interband transition region. This conclusion can also be deduced intuitively through the following arguments.

First, attenuation in the interband transition region was observed for both the anisotropic component I_{pp}^{aniso} and the SH intensity I_{sp} at $\phi=0$. If $\chi^{(2)}$ is enhanced through resonance with electronic transitions, it should give rise to an enhancement, not attenuation in the SHG signal. The mere fact that attenuation is observed should indicate that the dispersion in $\chi^{(2)}$ does not dominate the SHG behavior.

A comparison between the frequency dependence of the two anisotropic components, I_{pp}^{aniso} and I_{ss}^{aniso}, also supports the same conclusion. In Eqs. (16) and (17), I_{pp}^{aniso} and I_{ss}^{aniso} have exactly the same source terms containing the two second-order susceptibility components η (or ζ) and $\chi_{xxx}^{(2)}$. The frequency dependence of I_{pp}^{aniso} and I_{ss}^{aniso} should be very similar if the frequency dependence were dominated by $\chi^{(2)}$. However, as shown in Figs. 4 and 6, these two components bear no similarity in their frequency dependence. The difference in their frequency dependence can be accounted for by considering only the different SH radiation efficiency functions represented by $|F_c A_p|^2$ and $|A_s|^2$. It appears that depending on the light polarization condition, $\varepsilon(2\omega)$ can either attenuate or enhance the radiation efficiency of the SH signal. I_{pp}^{aniso} manifests a situation where the conditions are such that the radiation efficiency attenuates the SHG. But, in the case of I_{ss}^{aniso} the change in radiation efficiency enhances the SHG.

One unavoidably notices that the curves calculated with dispersion in the dielectric function only for the SH intensities do not match exactly with the experimental data. The discrepancy could be due to the inaccuracies in the dielectric functions. The other possibility is that the second-order susceptibility components may still have weak frequency dependence. Even though it does not dominate the SHG behavior, it may still affect the SH behavior.

The above discussions lead us to conclude that the sharp change in the dielectric function $\varepsilon(2\omega)$ induced by the interband transitions dominates the frequency-dependent behaviors of SHG in this energy region. Resonant enhancement in $\chi^{(2)}$ by the interband transitions or

other electronic transitions may still have some contribution but does not dominate the overall behavior of SHG.

Our understanding of the SH frequency-dependent behavior in this energy region is also consistent with the experimental observations made by Bradley *et al.*[12] on Ag(111) under UHV or immersed in an electrolyte solution. These authors have observed an enhancement in I_{sp} from the Ag(111) surface under both conditions. Since the dielectric function $\varepsilon(2\omega)$ is mainly a bulk electron property, it will not be much different whether the Ag surface is under vacuum or in a solution. The frequency-dependent behavior of SHG signal caused by $\varepsilon(2\omega)$ would then prevail in both environments. However, if the SHG peak is a result involving an occupied surface state, judging by the sensitivity of the surface state to adsorbate, the SHG peak is most likely to be greatly affected when the surface is immersed in a solution. Based on the dominant influence of $\varepsilon(2\omega)$ on the frequency dependence of the SHG, it seems to be unnecessary to invoke any electronic transitions involving surface states for the explanation of the observed SHG peaks in the Ag interband transition region.

VI. CONCLUDING REMARKS, A COMPARISON WITH Ag(110)

From analyzing the measured azimuthal-angle dependence and frequency dependence of SHG from a Ag(111) surface around the interband transition region by using the SMD model, we have provided strong evidences that the dramatic frequency-dependent changes of SHG at 3.9 eV is mainly due to the dispersion of $\varepsilon(2\omega)$. The pattern changes of both the angular dependence and frequency dependence can be adequately accounted for by the radiation efficiency of the generated SH signal from the solid surface into vacuum, which is governed by the dispersion of $\varepsilon(2\omega)$. There may have been resonant enhancement in the $\chi^{(2)}$'s by the interband transitions but such effect is small in comparison with the $\varepsilon(2\omega)$ effect. The radiation effect is so strong that for certain light polarization and azimuthal-angle conditions, the SHG is actually attenuated, rather than enhanced in this region.

In contrast, there are electronic transitions, e.g., surface state transitions, that do not affect ε but do enhance $\chi^{(2)}$. SHG in resonance with such purely surface electronic transitions would have different behaviors from the one coupled to the interband transitions. In Ref. 15, a resonant enhancement in the SHG intensity was observed on a Ag(110) surface. Analyses of the frequency dependence at different light polarization and different azimuthal angles have unambiguously proven, through symmetry selection rules, that the SHG peak is due to coupling of the fundamental light to a surface-state transition at 1.74 eV. Compared to bulk electrons, the number of electrons in the occupied surface state is too small to affect the dielectric function of the bulk. The radiation efficiencies of both the fundamental light and the SH light are only weakly frequency dependent near 1.74 and 3.48 eV, and, therefore, do not give a frequency-dependent response in the SHG signal. The breakdown of the inversion symmetry at the surface enables the second-order nonlinear optical process to be particularly sensitive to this surface-state transition. This gives a clear example that the observed SHG enhancement is purely caused by the enhancement of second-order susceptibility components through coupling to electronic transitions.

The surface-state transition enhances by resonance the surface $\chi^{(2)}$ but does not affect the ε. However, the interband transition is primarily a bulk electron property affecting the linear polarizability. Its effect on SHG can thus be best described by the change of the bulk linear response parameter ε.

ACKNOWLEDGMENTS

This work was supported by the National Science Foundation, MRL Program, under Grant No. DMR91-20668. Acknowledgment is made to the MRL Laser Facility at the University of Pennsylvania for the use of equipment. C.M.L. thanks Dr. Z. Charles Ying for stimulating discussions.

*Present address: Quadic Systems Inc., 29B Hutcherson Dr., Gorham Industrial Park, Gorham, ME 04038.

[1]F. Brown and R. E. Parks, Phys. Rev. Lett. **16**, 507 (1966).
[2]N. Bloembergen, R. K. Chang, S. S. Jha, and C. H. Lee, Phys. Rev. **174**, 813 (1968).
[3]Y. R. Shen, *The Principles of Nonlinear Optics* (Wiley, New York, 1984); Annu. Rev. Phys. Chem. **40**, 327 (1989).
[4]J. E. Sipe, D. J. Moss, and H. M. van Driel, Phys. Rev. B **35**, 1129 (1987).
[5]H. W. K. Tom, T. F. Heinz, and Y. R. Shen, Phys. Rev. Lett. **51**, 1983 (1983).
[6]H. W. K. Tom and G. D. Aumiller, Phys. Rev. B **33**, 8818 (1986).
[7]J. F. McGilp and Y. Yeh, Solid State Commun. **59**, 91 (1986).
[8]R. Murphy, M. Yeganeh, K. J. Song, and E. W. Plummer, Phys. Rev. Lett. **63**, 318 (1989).
[9]D. A. Koos, V. L. Shannon, and G. L. Richmond, Phys. Rev. B **47**, 4730 (1993).
[10]Z. C. Ying, J. Wang, G. Andronica, J.-Q. Yao, and E. W. Plummer, J. Vac. Sci. Technol. A **11**, 2255 (1993).
[11]S. Janz, K. Pedersen, and H. M. van Driel, Phys. Rev. B **44**, 3943 (1991).
[12]R. A. Bradley, R. Georgiadis, S. D. Kevan, and G. L. Richmond, J. Vac. Sci. Technol. A **10**, 2996 (1992).
[13]G. Petrocelli, S. Martellucci, and R. Francini, Appl. Phys. A **56**, 263 (1993).
[14]L. E. Urbach, Ph.D. thesis, University of Pennsylvania, 1992.
[15]L. E. Urbach, K. L. Percival, J. M. Hicks, E. W. Plummer, and H.-L. Dai, Phys. Rev. B **45**, 3769 (1992).
[16]T. F. Heinz, F. J. Himpsel, E. Palange, and E. Burstein, Phys. Rev. Lett. **63**, 644 (1989).
[17]K. Giesen, F. Hage, H. J. Riess, W. Steinmann, R. Haight, R. Beigang, R. Dreyfus, Ph. Avouris, and F. J. Himpsel, Phys. Scr. **35**, 578 (1987).
[18]A. Liebsch and W. L. Schaich, Phys. Rev. B **40**, 5401 (1989).
[19]H. G. Liljenvall and A. G. Mathewson, J. Phys. C **3**, S341

(1970).
[20]M. Otter, Z. Phys. **161**, 539 (1961); P. Winsemius, Ph.D. thesis, University of Leiden, 1973.
[21]P. Guyot-Sionnest, W. Chen, and Y. R. Shen, Phys. Rev. B **33**, 8254 (1986).
[22]J. Rudnick and E. A. Stern, Phys. Rev. B **4**, 4274 (1971).
[23]M. Corvi and W. L. Schaich, Phys. Rev. B **33**, 3688 (1986).
[24]W. L. Schaich and A. Liebsch, Phys. Rev. B **37**, 6187 (1988).